Optical tweezers

Manipulating the microscopic world

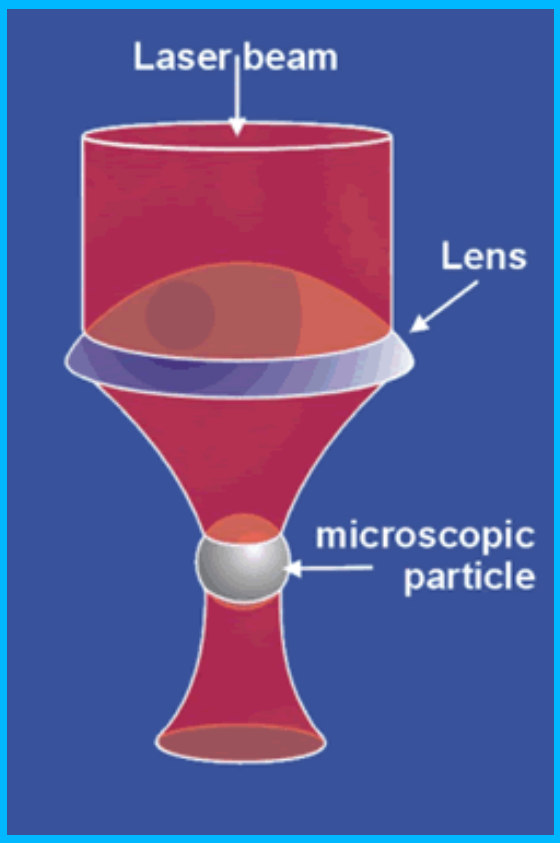

Name: Tom Lummen
Student nr.: 1209922
Date: May 2004
E-mail: T.T.A.Lummen@student.rug.nl

1. Introduction

Approximately four centuries ago, at the beginning of the seventeenth century, the first basic idea on which optical tweezers is based was born. A German astronomer, Johannes Kepler, famous for the discovery of the laws of planetary motion, noticed that tails of comets always point away from the sun. This implied that the sun exerted some kind of radiant pressure on the comets, or in other words, it suggested that light carries momentum. Nowadays, it is well known that light does indeed carry momentum; one photon of wavelength λ carries a momentum of $p = h/\lambda$, where h is Planck's constant. Thus, when a photon is absorbed, scattered or reflected by a particle, there is momentum transfer between the photon and the particle, in accordance with Newton's laws of motion. Although the corresponding optical forces experienced by the particle may only be ranging from femtonewtons to nanonewtons, they can be dominant in mesoscopic and microscopic systems. Optical tweezers have been applied in biological, physical and chemical systems, manipulating matter at length scales varying from micrometers to nanometers, as has been reviewed extensively elsewhere[1,2,3]. Biological applications of optical tweezers include the probing of the viscoelastic properties of DNA and cell membranes and the measurement of forces exerted by biological molecular motors. However, in this paper, the emphasis is on the applications of optical tweezers in physics, chemistry and materials science, and in particular on its possibilities and potential in micromechanics and microscopic engineering. The ability and versatile nature of the variety of optical traps, generally entitled optical tweezers, to remotely trap, move, assemble, cut and transform micoscopic particles and systems makes the optical tweezing technique an even fascinating as broad field of science. Starting from the theory and applications of conventional optical tweezers, this paper will expand its focus to the many variants of these conventional optical tweezers, after which the generation and applications of multiple simultaneous optical tweezers will be discussed.

2. Optical tweezers

Most of the early work in optical trapping is attributed to Arthur Ashkin. He built the first optical traps in the 1970's at AT&T Bell Laboratories. The first optical traps was built in 1970 and, like all optical traps, this so-called 'levitation traps' was based on the radiation pressure a particle experiences when in a laser beam[4]. Ashkin used the radiation pressure of a laser beam pointing upwards to balance the gravitational force pulling the particle downwards. When in balance, the particle would 'float' in mid-air due to the upward pointing optical force, somewhat similar to a tennisbal 'floating' on a vertical fountain. Somewhat later, in 1978, Ashkin had developed 'two-beam traps', which were based on the radiation pressure of two counterpropagating laser beams. Levitation and two-beam traps were precursors of the optical trap Ashkin and his colleagues would develop in 1986, the optical tweezers. This optical trap used only a single, strongly focused laser beam to trap a particle in three dimensions (3D). In this set-up, a Gaussian intensity profile laser beam (TEM_{00}, see fig. 1) is tightly focused using a high numerical aperture (N.A.) microscope objective, which can also be used for imaging the trapped particle. The theoretical description of optical tweezers is divided into two general approaches by the ratio (z) of the particle diameter (d) and the wavelength of the incident light (λ). In the so-called Mie regime, the particle size is very large compared to the wavelength of the incident light ($z = d/\lambda >> 1$) and the particle-light interaction can be described by simple ray optics. In the opposite limit, where the particle is very small compared to λ ($z = d/\lambda << 1$), wave optics are used to describe the interaction. This limit is also referred to as the Rayleigh regime. The theory for particles of sizes comparable to the wavelength of the incident light ($d \approx \lambda$) is non-trivial and still subject to debate.

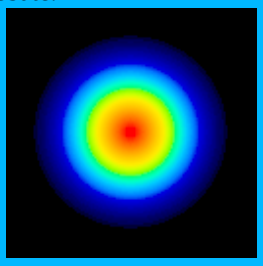

Figure 1: Intensity profile of a Gaussian laser beam. The light intensity decreases from the beam center outwards, from the red to the blue.[5]

In the Mie regime ($z = d/\lambda >> 1$) the trapping process can quite easily be understood by considering ray optics. The trapping process will be described in a qualitative manner in this section, a more quantitative description is given in the appendix. First consider lateral (x-y direction) trapping. A dielectric, transparent particle with a larger refractive index than its surroundings acts like a lens when placed in a laser beam. As depicted on the right hand side of fig. 2, the rays of light passing through the particle will be refracted. The particle thus exerts a force on the light, and consequently, in accordance with Newton's laws, will itself experience a force in the opposite direction. Since the laser beam has a Gaussian intensity profile (fig. 1), ray b is more intense than ray a, which means the forces the particle experiences due to these rays result in a net gradient force (F_{gr}) pointing in the direction of the beam

center. There is also a net scattering force (F_{scat}) pushing the particle in the direction of propagation of the light. In order to achieve also axial and thus 3D trapping, the Gaussian laser beam is focused by a high numerical aperture (N.A.) microscope objective, to create a steep axial intensity gradient in the beam. As is shown on left hand side of fig. 2, refraction of the focused beam gives rise to an axial, gradient force, F_{grad}, pulling the particle towards the focus of the microscope objective. The condition for stable 3D trapping in this set-up is the dominance of the axial gradient force F_{grad} over the scattering force F_{scat}, which is fullfilled for microscope objectives with sufficiently high numerical apertures, since F_{grad} is proportional to the objective's focusing angle.

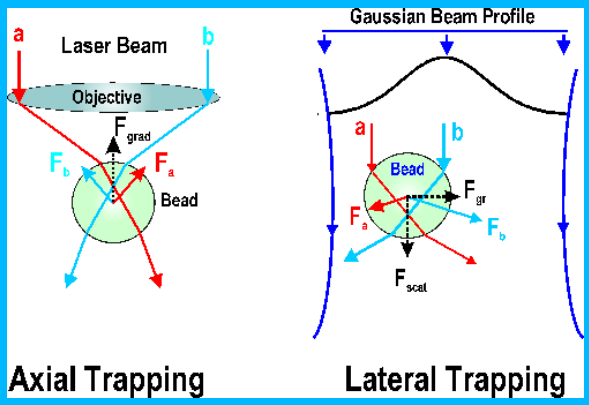

Figure 2: Optical trapping for particles in the Mie regime (z >> 1). The left hand side shows the principle behind axial trapping: the strongly focused laser beam is refracted by the particle, resulting in a gradient force (F_{grad}) pulling the particle towards the focus of the microscope objective. The right hand side depicts lateral trapping: due to the Gaussian intensity profile of the beam, the particle experiences a lateral gradient force (F_{gr}), pulling the particle towards the beam center, and an axial scattering force (F_{scat}), pushing the particle in the direction of propagation of the beam. Stable 3D trapping, in which case the axial gradient force dominates the scattering force ($F_{grad} > F_{scat}$), is achieved by microscope objectives with sufficiently high numerical apertures.[6]

In the Rayleigh regime ($z = d/\lambda << 1$) wave optics are used to describe the particle-light interaction.**Error! Bookmark not defined.** Since the particle is very small compared to the wavelength of the incident light, it is approximated by an induced point dipole, which interacts with the light according to the laws of electromagnetism. The particle experiences two forces due to the interaction with the incident light.

First, there is the scattering force, which pushes the particle in the direction of propagation of the light. Incident radiation can be absorbed and subsequently re-emmited (scattered) by the particle's atoms or molecules. The particle is then subject to two processes of momentum transfer; it receives momentum in the direction of propagation of the incident photon (during absorption) and in the opposite direction of the emitted photon (during re-emmision). Since the photon emmision by the atoms or molecules of the particles is isotropic, the time-averaged forces experienced by the particle due to the re-emmision of photons exactly cancel out, leaving only a net scattering force in the direction of propagation of the incident light:

$$F_{scat} = n_m \frac{\sigma \langle S \rangle}{c} \qquad (1)$$

where n_m is the index of refraction of the surrounding medium, <S> is the time-averaged Poynting vector, c is the speed of light and σ is the cross section of the particle, which for a spherical particle is given by

$$\sigma = \tfrac{8}{3}\pi (kr)^4 r^2 \left(\frac{n^2 - 1}{n^2 + 2} \right)^2 \qquad (2)$$

where n and r are the particle's refractive index and radius, respectively, and k is the wavevector of the incident light.

Secondly, the particle experiences a gradient force, which is nothing else than the Lorentz force acting on the induced dipole due to the incident electromagnetic field. The gradient force experienced by the induced dipole in an electric field $\vec{E}(\vec{r},t)$ is given by[7]:

(3)

$\nabla \times \vec{E} = 0$

(4)

The force the particle experiences is the time-

$I(\vec{r})$

$I(\vec{r})$

$I(\vec{r})$ is the light intensity and ε_0 the permittivity of free space, one obtains for the gradient force experienced by the particle:

$$\vec{F}_{grad}(\vec{r}) = \left\langle \vec{F}_{grad}(\vec{r},t) \right\rangle_T = \frac{\alpha}{2\varepsilon_0 nc} \nabla I(\vec{r}) \qquad (5)$$

Thus, the gradient force experienced by the particle is directed along the intensity gradient, towards the point of highest intensity, which in the case of a focussed Gaussian beam is the focal point of the microscope objective. As in the Mie regime, the requirement for stable 3D trapping is the dominance of the axial component of the gradient force over the scattering force. Again, this is achieved by a sufficiently large axial intensity gradient.

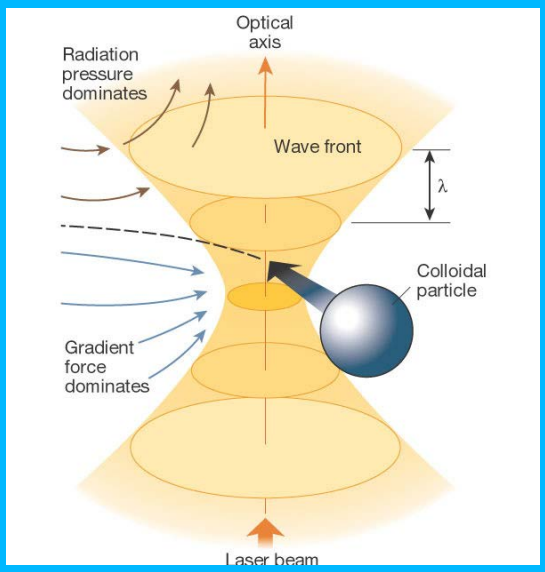

Figure 3: The principle of optical tweezers. If the axial gradient force dominates the radiation pressure, a particle is bound to the beam focus through an 'optical spring'. If, however, the radiation pressure dominates, a particle is pushes in the direction of propagation of the beam.1

In general, the optical trap can be thought of as an optical 'spring' connecting the particle to the point of highest light intensity, with the net force acting like a restoring force on the particle, when it is displaced from this focal point. This spring snaps however, when its corresponding restoring force (the axial gradient force) is overcome by the scattering force caused by the radiation pressure of the incident light. The principle of optical tweezers is summarized in fig. 3. The experimental set-up for optical tweezers is rather simple; a collimated Gaussian laser beam is guided into a microscope objective using a dichroic mirror. The use of the dichroic mirror allows for imaging the any trapped particles.

Optical tweezers have been used in many fields of science, ranging from biology and medicine to physics and materials science, in applications ranging from the optical manipulation of DNA to the movement of Bose-Einstein condensates. As mentioned before, these applications have been reviewed elsewhere1,[2,3], so this paper will only outline a few examples of their uses, where the emphasis will be on its applications in micro-mechanics and engineering.

2. I. Applications of optical tweezers

Conventional optical tweezers, as described above, have been used to measure the mechanical properties of a micromechanical spring, which was also fabricated using the strongly converging beam, through the non-linear process of two-photon-induced photopolymerisation[8]. Fig. 4 depicts this functional micromechanical spring in its equilibrium state (fig. 4.a.) and in a streched state (fig. 4.b.). The spring was converted into an oscillator by attaching one end to a colloidal bead and anchoring the other end to a glass substrate. Next, the spring was stretched by optically trapping and tranlating the bead connected to the spring. The spring constant was deduced to be 8.2 nNm^{-1} by releasing the bead from its displacement and measuring the damping of the oscillation (fig. 4.c.). Such micromechanical springs can be applied to the measurement of the mechanical properties of micrometer-sized objects.

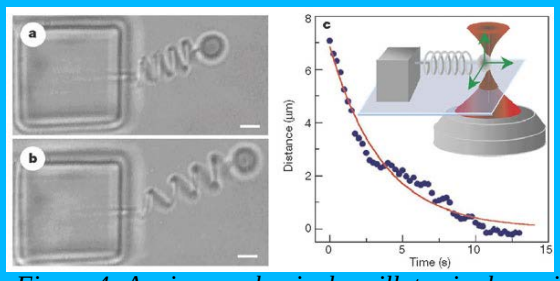

*Figure 4: A micromechanical oscillator is shown in its equilibrium state (**a**.) and in an extented state. (**c**.). The spring was stretched by optically trapping and moving the colloidal bead attached to one end of the spring, as depicted in the inset of **c**. The graph shows the restoring curve of the damped oscillation.8*

The two-photon polymerization method[9,10], where the optically induced polymerization of a resin is

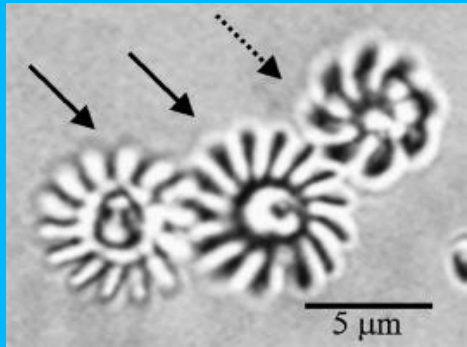

restricted to the focal volume of an incident laser, has also been applied to fabricate microstructures that rotate when trapped in a laser beam. These particles, shaped as a microturbine, were produced by moving the focus of a strongly converging laser beam along a pre-programmed trajectory.[11] Fig. 5 shows 3D models (fig.5.a,c) and actual photographs (fig.5.b,d,e) of such a microturbine from different angles. Although various shaped turbines have been investigated, the one in fig.5 has proven to be the most stable and efficient rotator.

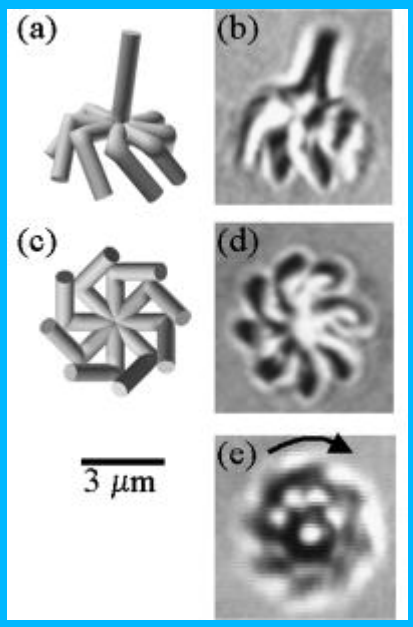

*Figure 5: 3D models and actual photographs of a optically driven microturbine. **a**. & **c**. 3D model drawing showing the ideal shape of the turbine from different perspectives. **b**. & **d**. Corresponding photographs of the actual microturbine, dispersed in acetone. In the photograph in **b**., the turbine is an arbitrary position, tumbling freely in solution, while in **d**. it is optically trapped using optical tweezers and held against the cover glass to prevent rotation, thus yielding a sharp photograph. **e**. Photograph of the turbine where it is optically trapped and spun by the incident laser light.11*

The dynamics of the turbine's rotation are quite straigtforward: incident photons are deflected by the helical structure of the turbine, and the change in their momentum results in a torque been exerted on the rotor. This torque is balanced by the viscous drag of the turbine, which sets the rotation speed. As one expects intuitively, the angular rotation speed is linearly proportional to the intensity of the incident light. Fig. 6 shows such a turbine driving a 'micromachine' consisting of two engaged cogwheels, which have also been fabricated through two-photon polymerization. By optically rotating the turbine, the two cogwheels are also rotated, showing the potential of such microturbines in complex micromachines.

Figure 6: Micromachine fabricated by the two-photon polymerization technique. The two engaged cogwheels indicated by the solid arrows are set into rotation by the optically induced rotation of the engaged microturbine, which is indicated by the dashed arrow. The cogwheels are rotating on axes that are fixed to the glass sample cover.11

Off course, many variations of and additions to the shape of these micromachines can easily be made using the same fabrication method. Combining this fabrication method with the shown light-induced rotation in laser tweezers creates a very broad and fascinating method for the creation of light-driven micromachines.

3. Unconventional optical traps

Next to the conventional optical tweezers described above, several optically trapping variants have been developed, based on different modes of light. Instead of using a Gaussian laser beam to optically trap a microscopic particle, Laguerre-Gaussian beams (LG beams) or superpositions thereof are employed to create new classes of optical traps with completely different properties, making them suitable for many potential applications in micromanipulation. Standard Gaussian modes of light can be transformed into the more exotic LG modes in various ways. The most straightforward way to make this transformation is by making use of computer-generated holograms, which essentially corresponds to imposing the desired phase profile on a Gaussian beam using a phase-only spatial light modulator (see fig. 9.a.). The computer-generated hologram technique is discussed in more detail in section 4.II. Another way to transform a Gaussian beam into an LG mode is by making use of so-called 'mode convertors'[12], which are composed of cylindrical lenses. Using these 'mode convertors', LG modes are obtained by the superposition of a certain number of phase-shifted Gaussian modes.

3.I. Optical vortices

For a collimated beam of light, the 3D wave equation is the paraxial wave equation, which can be solved in either the Cartesian or the cylindrical system of coordinates. The zero-th order Cartesian solution corresponds to the Gaussian beams used in conventional optical tweezers. These beams have a planar wavefront, meaning the light has a uniform phase in a plane tranverse to the direction of propagation. The solutions in cylindrical coordinates are the so-called Laguerre-Gaussian

modes, which are characterized by an axial, *l*, and a radial, *p*, index number (LG_p^l). The lowest order cylindrical solution, LG_0^0, is the same as the zero-th order Cartesian solution, the well-known Gaussian mode. The first order cylindrical solutions, LG_0^{+1} and LG_0^{-1}, correspond to modes with a 'doughnut' shaped transverse intensity pattern; a dark center surrounded by a ring of higher intensity. The field amplitude of a Laguerre-Gaussian mode LG_p^l in cilindrical coordinates is proportional to an associated Laguerre polynomial, L_p^l, through: $u_p^l(\rho,\phi,z) \propto \exp(-il\theta)L_p^l[2\rho^2/w(z)^2]$, where ρ is the radial distance to the beam axis, θ is the azimuthal angle around the beam axis, z is the axial distance from the beam waist and $w(z)$ is the beam diameter. An associated Laguerre polynomial is given by Rodrigues' formula:

$$L_p^l(x) = \frac{e^x x^{-l}}{p!}\frac{d^p}{dx^p}(e^{-x}x^{p+k}) \qquad (6)$$

For example, the polynomial characterized by indices $p = 2$ and $l = 1$ is given by the expression:

$$L_2^1(x) = \frac{e^x}{2x}\frac{d^2}{dx^2}(e^{-x}x^3) = \tfrac{1}{2}x^2 - 3x + 3, \qquad (7)$$

which is a second order polynomial with two 'nodes'; the function is equal to zero for two values of x. In general, an associated Laguerre polynomial $L_p^l(x)$ has is a *p*-th order polynomial which has *p* nodes. Basically, the radial index *p* indicates the number of dark nodes in the polynomial, so in general one can state that a Laguerre-Gaussian mode with $l > 1$ focuses to an intensity pattern consisting of $(p + 1)$ concentric rings, while an LG mode with $l = 0$ focuses to a bright central spot surrounded by *p* concentric rings of decreasing intensity (fig. 9.b.).

The most interesting aspect of these LG modes however, is their phase structure. As is clear from the field amplitude given above, the phase φ in such a mode is a function of the azimuthal angle (θ) around the optical axis: $\varphi(\boldsymbol{\rho}) = l\theta$, where $\boldsymbol{\rho}$ is the radial distance to the beam axis. This phase structure results in a corkscrew topology for a plane of uniform phase, while the formula $\varphi(\boldsymbol{\rho}) = l\theta$ governs the phase structure in a plane transverse to the direction of propagation, as represented by fig. 7.

Figure 7: Schematic representation of the phase structure in a transverse cut of a first order Laguerre-Gaussian mode. The figure shows the transverse phase structure in case of l = +1. Regions of identical phase are represented by regions of equal color, with the phase varying from 0 (blue) to 2π (red). In general, when going around the center in a circle, that is, as a function of the azimuthal angle (θ) around the optical axis, the phase advances an integer multiple (l) of 2π.[13]

The axial index *l* is an integer winding number, often referred to as the topological charge of the mode, which characterizes the winding speed of the phase around the optical axis. Positive values of the topological charge correspond to right-handed corkscrew modes, while negative topological charges describe left-handed corkscrew modes. The number of intertwined helices of which the phase front of an LG mode consists, is indicated by the absolute value of the topological charge. As is clear from fig. 7, the phase of the beam at its center is undefined, it can have any value between 0 and 2π. Therefore, LG beams with $l > 0$ are said to have a phase singularity at their optical axis, which is the cause of their 'doughnut' shaped transverse intensity patterns; presence of all phases results in complete destructive interference at the beam center.

Since the LG beam focuses to a ring of light surrounding a dark spot, it is suitable for trapping dark-seeking or photo-sensitive particles, that are repelled or damaged by conventional optical tweezers. Absorbing[14], reflecting[15] and low-dielectic-constant[16] particles have been trapped using LG beams. For strongly absorbing and reflecting particles, the scattering force becomes much larger than the gradient force due to the increased momentum transfer from the light to the particle. Consequently, absorbing and reflecting particles can be trapped two-dimensionally by a converging LG beam, but only if they are

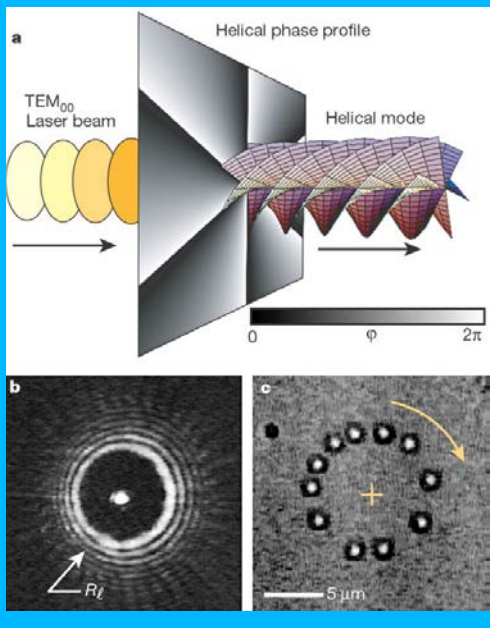

constrained in the direction of beam propagation (e.g. using a glass microscope slide). When displaced from the dark center of an LG beam, a trapped absorbing or reflecting particle experiences a scattering force, with one component directed towards the center and the other counteracted by some artificial axial constraint (fig. 8). For a reflecting particle, the situation is slightly more complicated, since the direction of the experienced force is dependent of the particle's surface geometry.

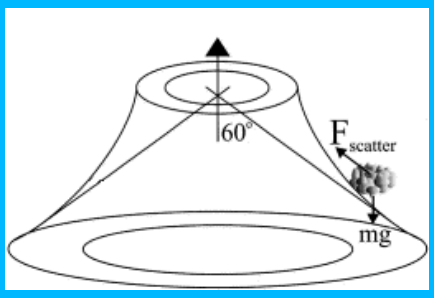

Figure 8: An absorbing or reflecting particle trapped in an LG beam experiences a scattering force due to momentum transfer. If the axial component of the scattering force is balanced by an artificial axial constraint and the LG beam is converging,, the particle can be trapped in 2D due to the lateral component of the scattering force, which directs the particle towards the zero-intensity beam center.15

For particles with a lower index of refraction than their surroundings (low-dielectric-constant particles), such as hollow glass spheres in water or water droplets in oil, it is possible to balance the axial component of the scattering force by an axial gradient force, since the scattering force is relatively small in this case. The use of strongly focusing microscope objectives thus enables 3D trapping of low-dielectric-constant particles using a converging LG beam, since the lateral component of the scattering force then directs the particle towards the dark focal spot of the 'doughnut' beam.

These Laguerre-Gaussian optical traps are generally referred to as 'optical vortices' or 'optical spanners', since they are capable of exerting torques as well as forces. About a decade ago, it was demonstrated12 that each photon in such a helical LG mode carries not only intrinsic spin angular momentum but also an orbital angular momentum of magnitude $l\hbar$. This orbital angular momentum acts as a tangential component of the linear momentum density and can be transferred to optically trapped particles[17,18].

*Figure 9: **a**. A helical phase profile is imposed on a conventional Gaussian laser beam (TEM_{00}) converting it into a helical LG mode. **b**. Instead of focusing to a bright spot of light, LG beams converge to an optical vortex. **c**. A single colloidal particle, 800nm in diameter, trapped on the circumference of an optical vortex is shown circulating the ring-like intensity pattern. The multiple exposure shows 11 successive stages of the particle's orbit at 1/6 sec. intervals.1*

Since the focus of an optical vortex consists of a ring-like intensity pattern, a small colloidal trapped particle of high index of refraction is drawn to the circumference of the high intensity ring. Due to transferred orbital angular momentum from the optical vortex photons to the particle, it circulates around the high intensity ring, as depicted in fig. 9.c. Such circulating particles entrain flows in the surrounding medium, that can pump and mix extremely small volumes of fluid. Using any of the techniques described below to create multiple, individually controlled optical vortices in specific arrays allows for the development of user-interactive microfluidics systems. Since the radius of an optical vortex increases with its topological charge17, the corresponding intensity pattern can be scaled to match the requirements for different applications.

However, since the rotation of particles using LG beams requires the transfer of orbital angular momentum from the light to the trapped particle, the particle must absorb a portion of the incident laser light, while it simultaneously must be transparent enough to allow stable 3D tweezing to occur. Furthermore, since the portion of the absorbed light can also induce damage to the trapped particle, this technique can only be applied to the limited range of non-photo-sensitive particles that fullfill this requirement.

3.II. Other optical rotators

Over the past decade, research into optically induced particle rotation concentrated itself in three other main approaches. The first of these approaches makes use of specifically shaped, prefabricated rotators, like the microturbine discussed in section 2. Although very promising for micromechanic applications using specifically shaped rotators, these methods are limited to these prefabricated objects. The second of these other approaches makes use of the birefringent nature of a trapped particle and its interaction with the incident light to induce rotation, while the third employs a rotating trapping pattern to rotate the trapped particle. In contrast to the first one, these last two other approaches, which are treated below, are not limited to objects of any specific shape.

3. II.a. Birefringent rotators

The second of the other methods was inspired by Beth's famous experiment[19], where he measured the torque exerted on a suspended quartz half-wave plate by incident circularly polarized light. In an microscopic analogy, this technique uses the fact that the polarization state of light passing through a birefringent particle changes, which results in an optical torque being exerted on the particle. The experimental set-up[20] used in this technique is that of conventional optical tweezers, expanded with a half-wave plate to enable rotation of the plane of polarization of the trapping beam, and a quarter-wave plate to allow for variation of the ellipticity of polarization of the initially linearly polarized light. The set-up is used to trap micrometer-sized particles of birefringent material (e.g. calcite), which can act as wave-plates due to their birefringent nature. For example, a 3 μm thick calcite particle acts as a λ/2 wave plate when using 1064 nm light. When passing through a birefringent medium, the ordinary and extraordinary components of the light travel at different speeds, determined by the different refractive indices they experience, n_o and n_e , respectively. The ordinary (O) and extra-ordinary (E) components of the light therefore will undergo different phase-shifts, which may result in a change in the spin angular momentum carried by the light. If the change in angular momentum of the light is nonzero, a corresponding torque is exerted on the particle, in accordance with the momentum-conservation law.

In general, an incident laser beam is elliptically polarized, meaning it has both linearly and circularly polarized components, and can be described by

$$E = \vec{x}E_0 e^{i\omega t}\cos\phi + i\vec{y}E_0 e^{i\omega t}\sin\phi \qquad (8)$$

where ϕ is a measure of the ellipticity of the light. The electric field of this elliptically polarized light can be separated in components parallel and perpendicular to the optic axis of the birefringent medium:

$$\vec{E} = E_0 e^{i\omega t}(\cos\phi\cos\theta - i\sin\phi\sin\theta)\vec{i} + E_0 e^{i\omega t}(\cos\phi\sin\theta + i\sin\phi\cos\theta)\vec{j} \qquad (9)$$

where θ is the angle between the optic axis of the birefringent medium and the fast axis of the quarter-wave plate used to produce the elliptically polarized light. The terms in eq. (7) correspond to the E- (first term) and O-components (second term) of the light, respectively. The phase shift induced by passage through the birefringent medium of thickness d is kdn_e for the E-component and kdn_o for the O-component of the light, where k is the wavenumber in free-space. Consequently the electric field emerging from the birefringent material will be20:

$$\vec{E} = E_0 e^{i\omega t} e^{ikdn_e}(\cos\phi\cos\theta - i\sin\phi\sin\theta)\vec{i} + E_0 e^{i\omega t} e^{ekdn_o}(\cos\phi\sin\theta + i\sin\phi\cos\theta)\vec{j} \qquad (10)$$

The angular momentum ***J*** of the light is given by:

(11)

where ε is the permittivity of the medium. From the change in angular momentum of the light due to the passage through the birefringent material, the torque per unit area exerted on the particle can be calculated:

$$\tau = -\frac{\varepsilon}{2\omega}{E_0}^2 \sin(kd(n_0 - n_e))\cos 2\phi \sin 2\theta + \frac{\varepsilon}{2\omega}{E_0}^2\{1 - \cos(kd(n_0 - n_e))\sin 2\phi \qquad (12)$$

The first thing to notice is the fact that the torque experienced by a non-birefringent particle is zero, since then n_o and n_e are equal. The first term in eq. (10) corresponds to the torque due to the linearly polarized component of the elliptically polarized light, while the second term represents the torque due to the change in polarization which occurs during passage through the birefringent particle. For linearly polarized light the second term is equal to zero since then ϕ = 0 or π/2, so the torque is proportional to *sin* 2θ. This means that the particle will always experience a torque as long as θ is non-zero, while it will experience no torque, that is, be in equilibrium if the angle θ is zero.

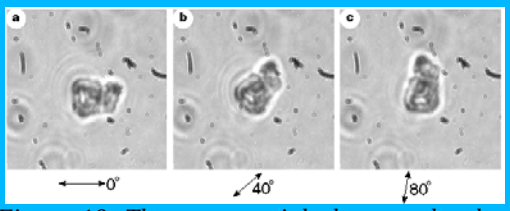

Figure 10. Three sequential photographs showing the alignment of a trapped calcite particle with the plane of polarization of the trapping light. The plane of polarization is rotated in steps of 40° between the successive photographs, by rotating the half-wave plate in the experimental set-up by steps of 20°.20

The particle will thus experience a torque unless its fast axis is aligned with the plane of polarization. Birefringent particles that are optically

trapped using linearly polarized light are thus always aligned in the particular orientation for which $\theta = 0$. When the plane of polarization is rotated using the half-wave plate in the set-up, the particle rotates correspondingly, exactly following the plane of polarization, as depicted in fig. 10. Modifying the set-up in such a way that it would enable the rotation of the half-wave plate at a preset speed would allow for rotating the particle at a predetermined frequency.

For a given ellipticity and intensity of the incident light, the second term in eq. (10) will be constant. For circularly polarized light ($\phi = \pi/4$), the second term reaches its maximum value while the first term vanishes, so a particle trapped in circularly polarized light will experience a constant torque. If the particle is dispersed in a viscous medium, this torque is balanced by the viscous drag torque, described by $\tau_D = D\Omega$ (where D is the drag coefficient), which will result in the particle rotating at constant angular speed Ω. Figure 11. shows a calcite particle trapped in elliptically polarized light. In this general case, the optical torque acting on the particle is a function of its orientation, so the rotation speed of the particles is not constant.

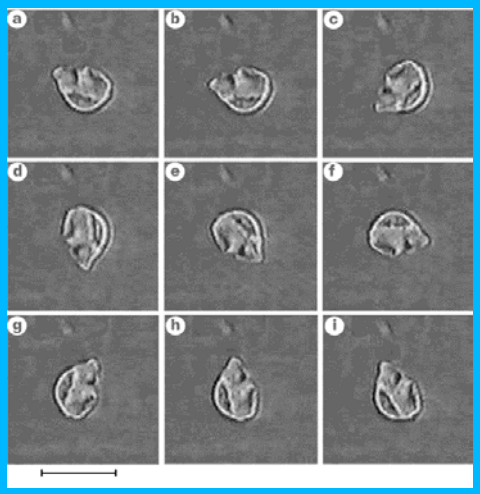

Figure 11: Nine sequential frames showing a calcite particle trapped in elliptically polarized light being rotated at a varying speed. The sequential images are 40 ms apart and the scale bar corresponds to 10 μm.20

This method has been used to rotate birefringent particles at constant frequencies of hundreds of hertz, the fastest rotation frequency reported20 was 357 Hz. The mayor drawback of this technique however is the fact that it is limited to the rotation of birefringent particles. Additionally, controlling the rotation speeds of the particles is a problem, since they are dependent on the viscosity of the surrounding fluid and since they are not constant when the particle is trapped with elliptically polarized light.

3. II.b. Rotating trapping patterns

The last main direction taken in the search for optical rotators is based on a rather simple idea. Instead of making the trapped particle rotate due to its interaction with the light through complex angular momentum transfers, particles are simply trapped in a rotating asymmetric trapping pattern, thereby inducing particle rotation.

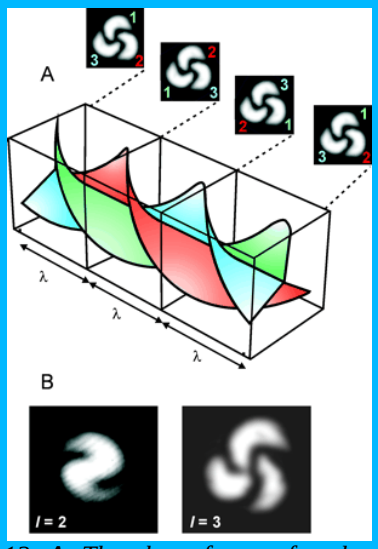

*Figure 12: **A**. The phase fronts of an $l = 3$ optical vortex can be visualized by a triple start intertwined helix, which repeats its azimuthal phase pattern every wavelength λ, but which only makes a full rotation after $l\lambda$. The insets show azimuthal intensity patterns resulting from the interference of the optical vortex with a plane wave at λ intervals, reflecting the triple helical structure. **B**. The interference patterns of $l = 2$ (left) and $l = 3$ (right) optical vortices with plane waves, consisting of 2 and 3 spiral arms, respectively.*[21]

This technique makes use of Laguerre-Gaussian modes of light, which are characterized by their topological charge index l, as discussed above. This integer number l denotes the number of complete 2π-cycles the phase undergoes when going around the circumference of the mode. For example, an $l = 2$ or $l = 3$ optical vortex can be represented by double or triple start helical phase fronts, respectively (fig. 12.A.). As mentioned above, the phase in a transverse cut through an optical vortex is dependent on the azimuthal angle through $\varphi(\rho) = l\theta$. By interfering an optical vortex with a conventional plane wave, this azimuthal phase variation can be transformed into an azimuthal

intensity variation, resulting in a intensity pattern consisting of *l* spiral arms (fig. 12.B.).

The experimental set-up used in this technique is again a conventional optical tweezers set-up, in this case expanded with a computer-generated hologram an interferometer (fig. 13). A standard plane wave is incident on a computer-generated hologram (see section 4.II), which splits the incident beam in a plane wave and an optical vortex of topological charge *l*. The optical vortex and the plane wave are then separately guided into different arms of an interferometer, after which they are recombined to form one trapping beam.

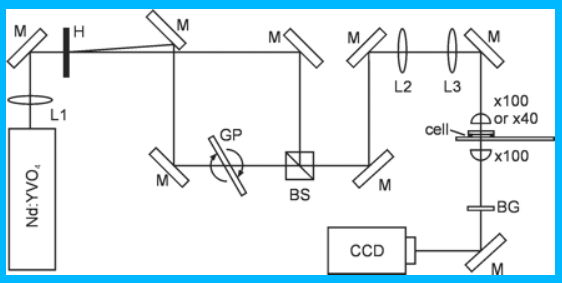

Figure 13: A conventional optical tweezers set-up expanded with a hologram (H) and an interferometer. The optical vortex and the plane wave emerging from the hologram are guided into different arms of an interferometer before being recombined into one trapping beam. The interferometer allows for variation of the relative path lengths of the two interfered beams, and therefore enables rotational control of the trapping pattern. Symbols: L, lens; M, mirror; GP, glass plate; BS, beam splitter; x100 or x40, microscope objectives; CCD, camera; BG, infrared filter.21

The optical path length in one of the arms of the interferometer can be varied by rotating the glass plate, which results in the rotation of the interference pattern of the vortex and the plane wave around the beam axis. This can be understood by considering the following analogy. Imagine cutting a thick rope consisting of *l* intertwined cords and viewing its cross-section. As the position of the cross-section is translated along the length of the rope, each of the individual intertwined cords rotates around the rope axis. This is similar to what happens when varying the optical path length of one of the interfering beams. The point where the optical vortex and the plane wave are combined to form one trapping beam corresponds to the position of the cross-section, while varying the optical path length of the optical vortex is analogous to moving this position along the length of the rope. The particles in the trapping beam are drawn to the regions of highest intensity (the spiral arms in the interference pattern) by the gradient force, so as these regions are rotated around the beam axis through variation of the vortex' path length, so are the trapped particles. Fig. 14 shows two silica spheres (fig. 14.A), a glass rod (fig. 14.B) and a Chinese hamster chromosome (fig. 14.C) being rotated with this technique, using the interference pattern of an $l = 2$ optical vortex and a plane wave.

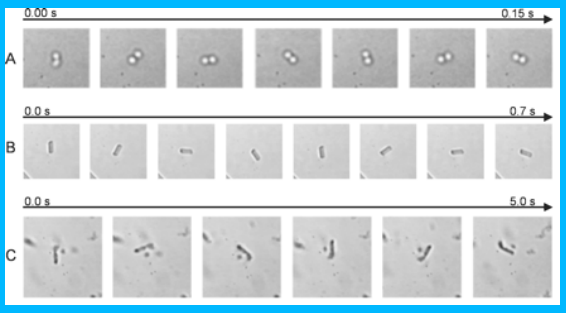

*Figure 14: Optical rotation of trapped objects in the interference pattern of an l = 2 LG beam and a plane wave. **A**. 7 sequential photographs showing rotation of two silica spheres trapped in the spiral arms of the interference pattern at a frequency of 7 Hz. **B**. Rotation of a 5-μm-long glass rod shown in 8 sequential frames. **C**. Similar rotation of a Chinese hamster chromosome. The elapsed time in seconds is indicated above each set of frames by the scaling arrow.21*

This technique does not make use of a specific property of the trapped particle to induce optical rotation, which makes it in principle applicable to any object that can be optically trapped using conventional optical tweezers. The technique provides a very simple way of controlling both the sense and speed of rotation through the controlled sense and speed of rotation of the glass plate in the interferometer. Additionally, the possibility of using optical vortices of different topological charges makes the technique applicable to differently shaped objects and groups of objects, which are however, limited to objects and groups of objects having a similar rotational symmetry. The drawback of this technique is the fact that the rotation speed of the particles is limited by the requirement that they stay stably trapped within the intensity pattern, which results in the limitation of the maximum rotation speed to about 5 Hz.

3. III. Optical bottles

The optical vortices discussed above have thus far only succeeded in 2D optical trapping of dark-seeking objects. 3D trapping of these objects has only been achieved by making use of artificial axial constraints. In order to optically trap such dark-seeking particles in 3D, a new type of beam is required, which has its dark focus surrounded by regions of higher-intensity in all directions. The

intensity cross-section at the focus of an optical bottle beam differs from that on either side of the focus, meaning the beam is not structurally stable. Structurally unstable beams can be created by superposing two structurally stable beams whose relative phase varies during propagation. This is the case in the vicinity of a beam waist, where two superposed LG modes propagate with the same wave number, but with a different Gouy phase[22]. The Gouy phase, $\Psi(z)$, of a LG mode enters its electric field as a factor $exp[-i\ \Psi(z)]$, where $\Psi(z) = (2p+l+1)arctan(z/z_R)$, z is the distance from the beam waist and z_R is the Rayleigh range of the beam. The Rayleigh range of a beam is defined as the axial distance from the beam waist to the point where the beam diameter is a factor $\sqrt{2}$ larger. When properly adjusting the intensities (fig. 15) and relative phases of an $l = 0$, $p = 0$ and an $l = 0$, $p = 2$ LG mode, they interfere destructively at their common focus, resulting in zero intensity at the focal point.

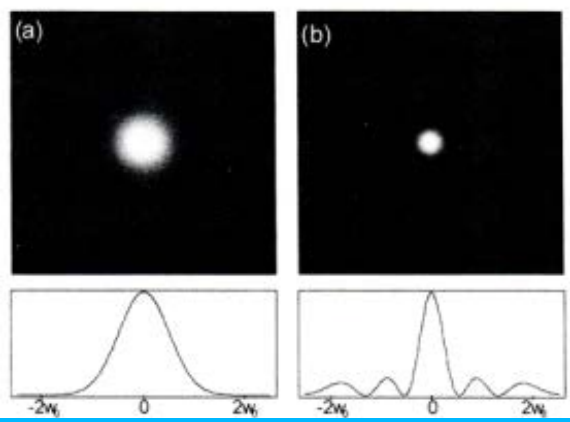

Figure 15: Transverse intensity cross-sections and profiles of ***a****. an l = 0, p = 0 LG mode and* ***b****. an l = 0, p = 2 LG mode. w_0 denotes the beam waist.*[23]

On either axial side of the beam focus, the two modes interfere constructively, resulting in an optical potential well for dark-seeking objects at the beam focus. The rate of change of the relative phase between the two beams determines the size of the optical bottle, which can be adjusted by using LG modes which differ more in their radial index p. Fig. 16 depicts the calculated intensity profile of the optical bottle in three directions. Although the optical potential well is not spherically symmetric, it is surrounded by regions of higher intensity in all directions.

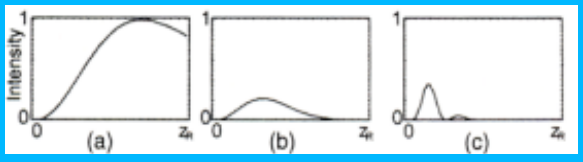

Figure 16: Intensity profiles of the optical bottle beam. The graphs show the spatial intensity distribution from the center of the focal point, ***a****. along the direction of propagation,* ***b****. along the direction of minimal intensity and* ***c****. along the radial direction. The horizontal scale depends on the degree of focusing.*[23]

Although an optical bottle beam has been created using this method23, thus far there have been no reports of particles beam trapped using this technique, which appears to still be in its research stage. Still, an optical bottle beam has potential applications such as the 3D optical trapping of low-dielectric-constant particles and cold atoms.

4. Multiple optical traps

After the succesfull implementation of the single optical traps described above, it was quite obvious that expanding the number of single tweezers without the use of multiple laser sources would open up a whole new world of interesting possibilities. Since then, a number of techniques have been developed that actually permit simultaneous trapping of multiple particles. These various techniques are discussed and compared below.

4. I. Scanned time-shared optical tweezers

The first method that succeeded in optically trapping multiple particles simultaneously, is the so-called scanned or time-shared optical tweezers technique. In this technique[24,25], a single laser beam is scanned over the several trapping sites periodically. Despite the fact that each trapping site is only illuminated part time, the time-averaged optical force experienced by a particle located at a trapping site is strong enough to ensure stable trapping, provided the scanning speed of the laser is sufficiently rapid. The set-up used in such a time-shared trapping experiment is schematically depicted in fig. 17. The trapping laser beam is deflected by two mirrors, which are operated by a computer-controlled driver, after which it passes through two lenses (L1 and L2), employed to match the beam diameter to that of the microscope objective's numerical aperture. Rescaled by the lenses, the laser beam is reflected into the microscope objective by a dichroic mirror (DM), where the objective lens focuses the beam into an optical trap. Entrance of the beam into the objective along the objective's optical axis, will result in an optical trap being formed in the center of the objective's focal plane. Entrance of the beam at an angle will result in an optical trap located proportionally off-center. Using these physics, the computer-controlled galvano mirrors allow for the necessary scanning of the optical tweezer through

the focal plane of the objective lens in the desired patterns. The dichroic mirror allows for imaging of the focal plane using a CCD camera.

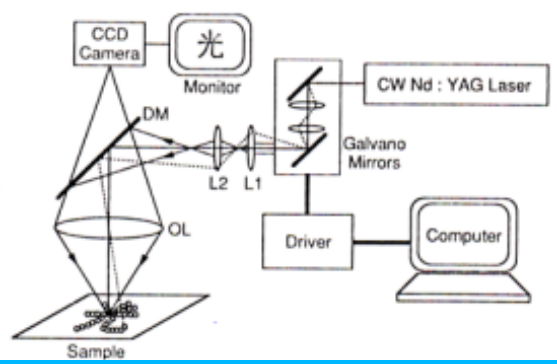

Figure 17: Schematic diagram of the set-up used in the time-shared laser scanning technique. The two computer-adressed galvano mirrors provide controlled scanning of the optical tweezers through the focal plane of the objective lens (OL).24

This method was used to trap multiple particles configured in various spatial24, of which one is depicted in fig. 18. Using the time-shared trapping technique, 46 polystyrene latex spheres, about 2 μm in diameter, are optically trapped in the pattern forming the Chinese character for light.

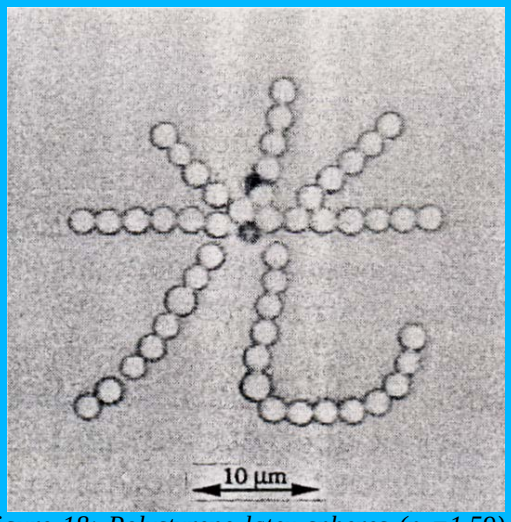

Figure 18: Polystyrene latex spheres (n =1.59) in ethylene glycol (n = 1.43) are spatially trapped into a pattern, forming the Chinese character for light.24

Next to the optical trapping force, a scanned time-shared laser beam also exerts a driving force on the particles it traps. As discussed above, a particle with a higher refractive index than its surrounding medium is attracted to the focal spot of an optical trap by a gradient force. This attractive force is schematically plotted in fig. 19.a. as a function of the distance between the particle's center and the focal spot. No force is exerted on the particle when it is centered exactly in the focal spot of the optical trap. When displaced from this equilibrium position however, the particle experiences an attractive force directed towards the equilibrium position, which as a function of displacement first increases and then decays. Due to the symmetry of the curve, the net force experienced by the particle is zero when the focussed beam is scanned across (as indicated above the curve), since it is given by an integral of the curve. In reality however, the particle is initially displaced to the left by the attractive trapping force, which approaches from the left, untill the particle is in the equilibrium focal spot of the optical trap. Therefore, the left half of the curve is compressed, as shown in fig. 19.b. Similar reasoning explains the expansion of the right half of the curve, since the particle is dragged along with the trap as it moves to the right. Integration of the resulting asymmetric curve shows the particle experiences a net force in the scanning direction of the optical trap, which is the so-called driving force mentioned above.

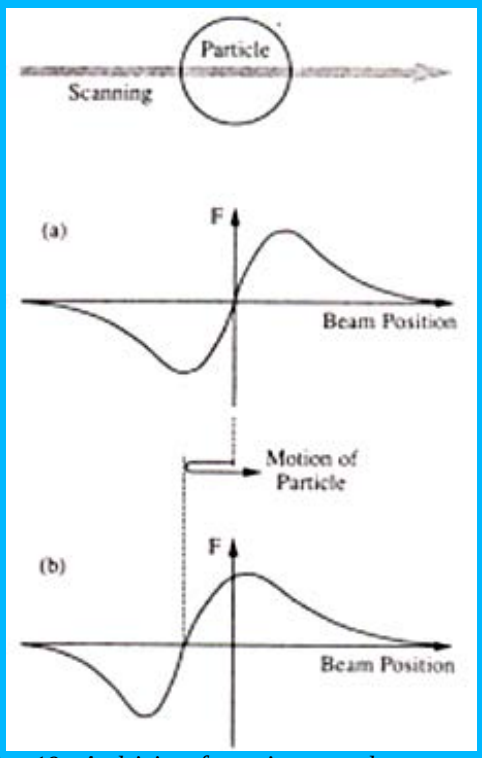

Fig. 19: A driving force is exerted on a particle when an optical trap is scanned across. The scanning direction is indicated above, positive radiation forces are in the scanning directing, while negative forces are in the opposite direction. ***a****. The optical force exerted on a fixed particle plotted against the relative displacement of the*

*optical trap. **b**. The same optical force, as exerted on a particle that is free to move. In this case, the particle experiences a net force, given by an integration of the curve, in the scanning direction.24*

In these scanning optical traps, where the laser beam is periodically scanned across the desired trapping pattern, the driving force exerted on the particles thus drives them continuously. Figure 20. shows the particle flow of 1μm diameter, polystyrene latex spheres induced in this way. The incorporation of a slightly larger particle in the circular pattern allows for the visualisation of this driving flow. From the sequential images a particle flow velocity of 12.2 μm/sec was calculated24, at a scanning speed of 642 μm/sec. The particle flow velocity is dependent on the scanning speed, intensity and focusing angle of the laser beam, the frictional forces between the particle and the quartz plate sustrate and on the viscous resistance of the suspension medium. The particle flow velocity decreases as the scanning speed of the laser is increased, since the mechanical response of the particle is lower at high scanning speeds due to its inertia. No matter what the scanning speed, the particle may always flow slightly. To eliminate particle flow in full, alternating scanning directions need to be employed.

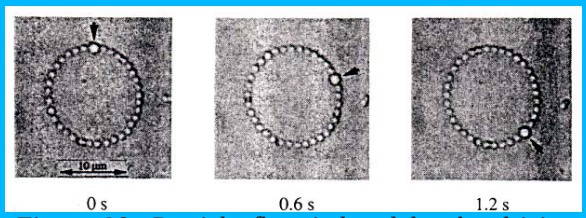

Figure 20: Particle flow induced by the driving force exerted by the scanned laser beam. The sequential images (0.6 sec apart) visualize the particle flow through the incorporation of a slightly larger particle, marked by the arrow, in the circular pattern of 1μm diameter polystyrene latex spheres suspended in 1-pentanol.24

In short, the scanned time-shared optical tweezing technique can be employed to create spatial trapping patterns, which can be configured dynamically through computer control of the scanning mirrors. Similarly, single trapped particles can be transported across arbitrary paths. This technique however is restricted to generation and dynamic recongifuration of trapping patterns and single optical traps in 2D. Furthermore, the patterns of optical traps that can be obtained are limited in extent and complexity by the time required to ensure stable trapping by the multiple time-averaged optical potential wells. Also, the obtainable trapping patterns seem to be limited to patterns consisting of connected lines of particles.

4. II. Holographic optical tweezers arrays

In a completely different approach to create an array of optical tweezers, a computer-designed diffractive optical element (DOE) is used to split a single Gaussian laser beam into multiple separate beams. Each of these separate beams is focused into an optical trap using a strongly focusing microscope objective.

The set-up for creating these so-called holographic optical tweezers (HOT) is schematically depicted in fig. 21. As discussed above, any beam passing through the objective's back aperture (point B in fig. 21) will be focused into an optical trap. If the beam follows the optical axis of the objective, that is, if it enters the objective at an angle of 0° with respect to the optical axis, it will form an optical trap in the center of the objective lens' focal plane. If, by contrast, the beam enters the objective an a nonzero angle, the resulting trap will be offset from the center of the focal plane. Slightly converging or diverging beams come to a focus up- or downstream of the focal plane, respectively.

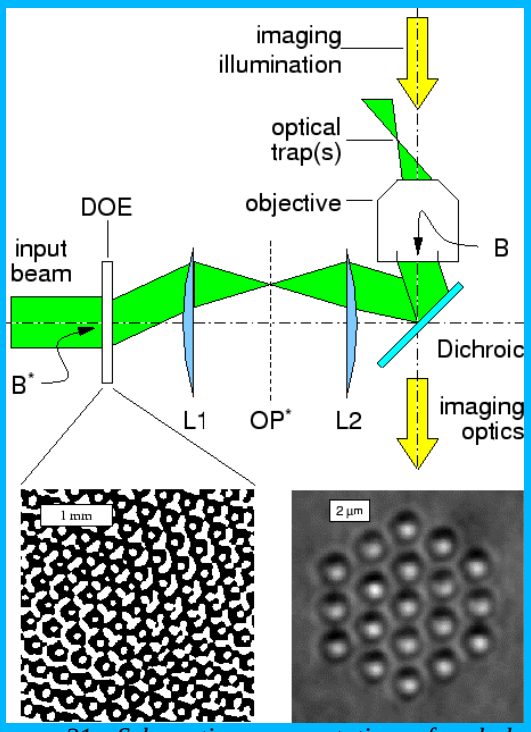

Figure 21: Schematic representation of a holographic optical tweezers array. The input beam is split into multiple beams by the DOE, which are then separately transferred to a strongly focusing objective by two lenses L1 and L2 and a dichroic mirror. Each separate beam is focused into an optical trap by the objective. The lower left panel shows the phase pattern (dark regions correspond

to a phase-shift of π radians) that resulted in the array of optical traps used to trap 1 μm diameter silica particles in the lower right panel. ***Error! Bookmark not defined.***

Lenses L1 and L2 in fig. 21 form a telescope, which creates a conjugate point, B*, to the center of the objective's back aperture. Basically, the telescope creates an image of the objective's back aperture, centered at the conjugate point B*. Any beam passing through point B* also passes through point B and will thus form an optical trap. By placing a DOE at point B*, a single laser beam can be split into any desired distribution of beams, each of which thus forms a seperate optical trap in the focal volume of the objective's lens. The dichroic mirror used to direct the beams into the objective allows light of different wavelengths to pass through undisturbed, which creates the possibility of imaging any trapped particles. Fig. 21 also shows a computer-generated binary phase hologram pattern, which splits a single beam into multiple separate beams, along with a photomicrograph of colloidal particles trapped in the resulting pattern of optical traps.

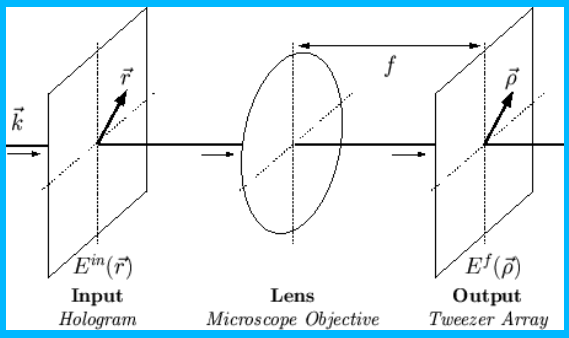

Figure 22: Schematic representation of the relationship between the beam wavefronts in the input and focal planes. Monochromatic light (wavevector $\vec{k}$) is incident on the input plane. A microscope objective of focal length f focusses the Fourier transform of the incident light's wavefront into an optical tweezers array. ***Error! Bookmark not defined.***

The bottleneck in creating arbitrary arrays of optical tweezers in the focal volume of the objective is the calculation of the appropriate wavefront of the light at the plane of the DOE, needed to obtain the desired wavefront in the focal volume. As depicted in fig. 22., for a planar array of optical traps, the intensity distribution of laser light in the focal plane, $I^{f}(\vec{\rho})$, is dependent on the electric field of the light incident on the input plane. The electric field at the input plane consists of the real-valued phase ($\phi^{in}(\vec{r})$) and amplitude ($A^{in}(\vec{r})$) functions:

(13)

The wavefront in the focal plane, $E^{f}(\vec{\rho})$, has a similar form,

, (14)

[illegible] denote the Fourier transform and inverse Fourier transform of function *X(r)*, respectively.

Creation of the desired wavefront in the focal plane requires the appropriate wavefront in the input plane. Lasers, however emit only a fixed [illegible] $E_0(\vec{r})$ i $E^{in}(\vec{r})$ [illegible] $E_0(\vec{r})$ [illegible] amplitude of the laser beam results in diverting power from the beam, this leads to a decrease in trapping efficiency, which is undesirable. Fortunately, this can circumvented by setting $A^{in}(\vec{r}) = A_0(\vec{r})$ and only modulating the phase of the input beam to obtain the desired trapping wavefront. The DOE, also referred to as the phase hologram or kinoform, induces the appropriate phase modulation, which transforms the input beam $E_0(\vec{r})$ into the necessary wavefront

(15)

where $\phi^{in}(\vec{r})$ is the modulated phase profile.

There are several techniques capable of imposing the necessary phase modulation, as will be discussed below, but the calculation of the needed phase hologram is not particularly straightforward since the corresponding system of equations has no analytical solution. Nevertheless, several iterative optimization algorithms have been developed[26,27,28], to be able to calculate the phase modulation necessary to create any desired trapping structure.

Once it is known, there is the need to impose the modulated phase profile onto the input laser beam, using a kinoform. There are several techniques to design an appropriate kinoform, and they can be divided into two classes. First there are the static

kinoforms, consisting of microfabricated phase modulating optical elements and second are the dynamic kinoforms, consisting of dynamically reconfigurable phase modulators.

4. II.a. Static holographic optical tweezers arrays

There are basically two ways of recording a static phase profile in an optical element. First there are the so-called photorefractive holograms, in which controlled variations of the index of refraction of a dielectric are used to impose the desired phase modulation. Fabrication of these photorefractive holograms involves patterned photo reduction onto holographic plates, thus obtaining amplitude holograms, followed by development and bleaching of these amplitude holograms to phase holograms[29]. Although these photorefractive holograms offer the greatest flexibility and lowest cost for kinoform production, this technique is still in the research stage.

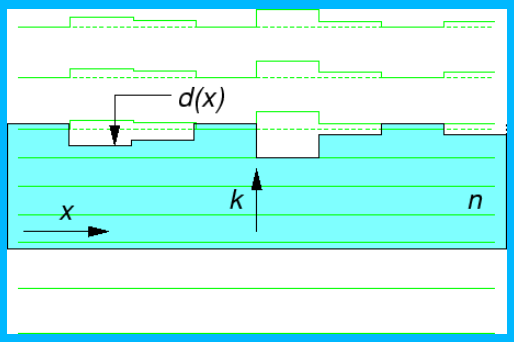

Figure 23: Imposing a phase profile with the surface patterning technique. An incident plane wave, with a uniform phase wavefront, acquires a spatially modulated phase wavefront due to different portions of the beam covering different pathlengths through the dielectric material.Green lines indicate the spatial phase profile as the light propagates through the material.26

The second technique available to encode phase in a static kinoform is surface patterning. The principle of this technique relies on the fact that light propagates faster in air than in a dielectric material. When entering a dielectric material of refractive index *n*, an electromagnetic wave of frequency ω and wavelength λ is slowed down to a propagation speed of $c/n(\omega)$, where *c* is the speed of light in vacuum. By pattering the surface of the dielectric material, the optical path length through the material is spatially modulated, thereby inducing a spatially modulated phase profile, as depicted in fig. 23. The relative phase at position $\vec{r}$, $\phi^{in}(\vec{r})$ is proportional to the surface relief at $\vec{r}$, $d(\vec{r})$:

(16)

Imposing a spatial phase profile through reflection off of a spatially patterned surface results in a similar equation, where with respect to eq. (14) the factor $(n-1)$ is replaced by a factor 2.

Implementation of the surface patterning is achieved through microfabrication techniques, or more specifically, using photolithographic techniques. The basic steps in the creation of a spatially patterned surface using photolithography are depicted in fig. 24. First the surface of the fused-silica substrate is polished and protected by a thin layer of chromium and a layer of positive photoresist (fig. 24.a.).

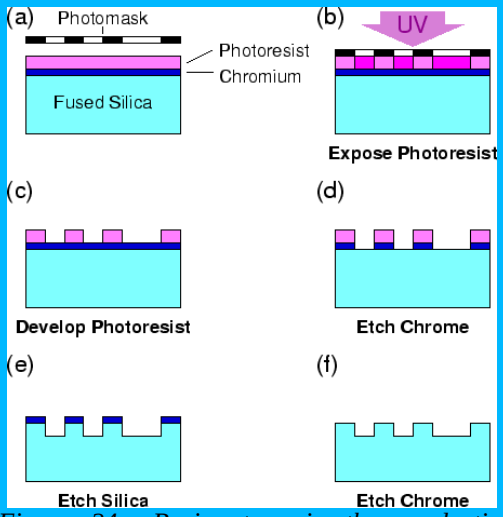

Figure 24.: Basic steps in the production of spatially textured dielectric materials.[26]

Next a photomask is placed in contact with the photoresist, protecting the desired spatial pattern from subsequent UV irradiation (fig. 24.b.). After removing the photomask, the exposed regions of photoresist are dissolved away, leaving regions of the chromium layer unprotected (fig. 24.c.). The revealed chromium layer regions are etched away by an acid wash, exposing parts of the silica substrate (fig. 24.d.). Next, the unprotected silica sections, and the remaining photoresist, are subject to attack by fluoride ions in a process called reactive ion etching. The unprotected regions of silica are removed at a certain rate (*x* nm/sec.), depending on the etching solution's composition, untill the etched regions reach the desired depth (fig. 24.e.). Finally, the remaining chromium is removed to obtain the spatially profiled kinoform (fig. 24.f.).

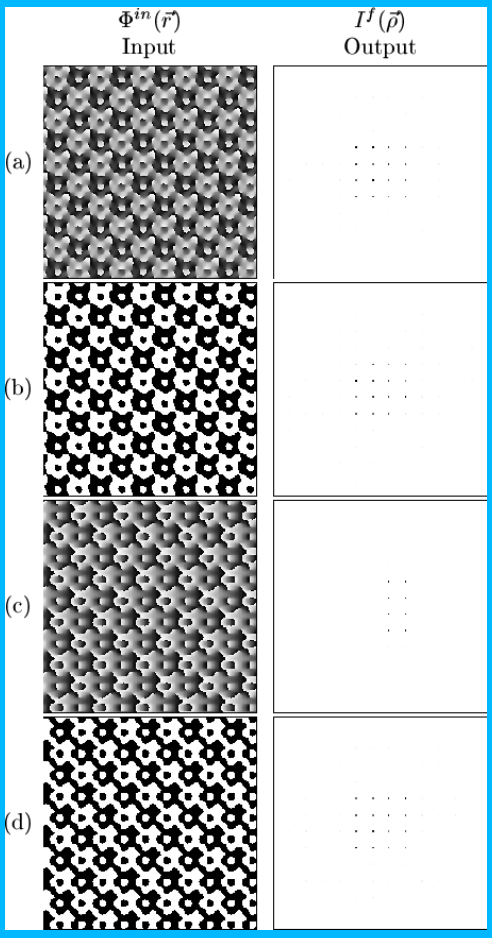

Figure 25: ***a.*** *A continuous phase hologram (left) encoding a 4x4 array of optical traps (right).* ***b.*** *The binary analogue of the hologram in (a) results in an array with missing traps.* ***c.*** *A continuous phase hologram resulting in a 4x2 optical trap array.* ***d.*** *The binary analogue of the hologram in (c) does create the desired 4x4 array of optical traps.26*

To incorporate multiple gradations of depths and thus produced more complicated patterns, the etching process can be repeated using different photomasks. This, however, does make the process quite time consuming. Consequently, the most straightforward kinoforms make use of only two gradations of phase delay and are therefore called binary holograms. Binarization imposes inversion symmetry on the resulting trapping pattern and thus limits the trapping geometries to inversion symmetric structures. Binarization may also induce some additional undesired side effects due to the interference between two sides of the pattern, as depicted by fig. 25.a,b. These side effects are supressed by employing a phase mask calculated to encode only half of the array (fig. 25.c,d.). Although their name suggests otherwise, static kinoforms do posses some form of reconfigurability: rotation of the kinoform around its optical axis equivalently rotates the resulting trapping pattern and individual tweezers can be removed from the pattern by blocking their beams in the plane depicted by the line OP* in fig. 21.

These static kinoforms have been employed to create both square and triangular arrays of up to 400 optical tweezers26, however it seems the method increases rapidly in complexity and thus decreases in feasibility when one is interested in three dimensional, rather than two dimensional structures. It is possible however, to configure the the wavefronts of the single tweezers to create any of the variants discussed above by modification of the algorithm28.

4.II.b. Dynamic holographic optical tweezers arrays

A new chapter in holographic optical tweezing was added when dynamically reconfigurable spatial light modulators (SLMs) became available. An SLM typically consists of a computer adressed liquid crystal display (LCD), which is modified to modulate only the phase of incident light. The pixelated SLM induces a computer-controlled amount of phase delay at each pixel in an array. This phase modulation is again achieved by varying the local optical path length, this time by the controlled local orientation of the molecules in the LCD through a computer. By dynamically reconfiguring these computer-designed kinoforms, the resulting trapping patterns can also be dynamically reconfigured. An appropriate sequence of phase holograms can encode the independent movement of multiple trapped particles or the transformation of one trapping configuration into another, provided the individual traps are only slightly displaced between successive trapping patterns27,28,30. This, of course, is only possible if the corresponding necessary phase modulations have been pre-calculated using any of the iterative algorithms referred to above. Fig. 26. demonstrates the potential of such a dynamically reconfigurable optical trapping set-up. It shows 26 colloidal silica spheres, 0.99 μm in diameter, suspended in water and trapped in an pentagonal configuration (fig. 25.(a)), being moved in 38 steps small steps to ultimately form a circular pattern (fig. 25.(c)). Each step consists of replacing the previous kinoform with one whose traps are slightly displaced with respect to their previous position.

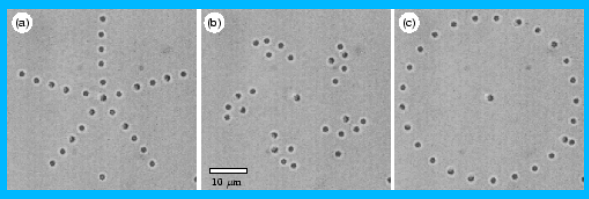

*Figure 25.: Dynamic reconfiguration of 2D-trapping patterns. The original pentagonal pattern of 26 trapped silica spheres (**a**) is gradually transformed into a circular pattern (**c**) in 38 steps, through many intermediate patterns, of which only one, after 16 steps (**b**), is shown.28*

Using this method, translation of particles at speeds up to 10 μm/sec. have been reported28. Although comparable planar motions have been reported using scanned time-shared optical tweezers (as discussed above), the continuous illumination of holographic optical traps offers some advantages. For example, dynamic holographic optical traps can support more extensive patterns in both space and number of traps due to fact that the time-shared arrays require the periodic releasing and retrieving of trapped particles. Additionally, dynamic HOTs use lower peak intensities for trapping, which makes this method less damaging for photo-sensitive samples.

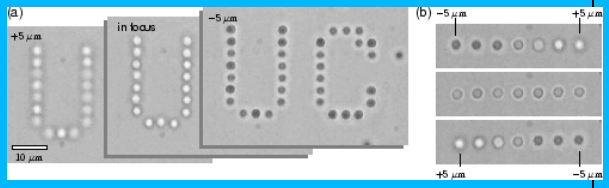

*Figure 26: Three dimensional motion of trapping patterns. **a.** 34 silica spheres 0.99 μm in diameter trapped in three different, single axial planes. The spheres' appearance changes as they are translated relative to the focal plane. **b.** 7 trapped silica spheres, simultaneously and independently moved through 7 different axial planes, relative to the focal plane.28*

So far, only the generation 2D-patterns of optical traps have been discussed. However, as mentioned above, a slightly diverging or converging input beam would come to a focus correspondingly down- or upstream of the focal plane. Divergence or convergence can be induced in a laser beam using a Fresnel lens, however, such divergence or convergence also can be incorporated in any individual trap of a pattern by simply incorporating the effect of Fresnel lens into the existing kinoform. Fig. 26. shows silica spheres being moved both coherently and independently through multiple axial planes in this way.

Next to inducing divergence into a laser beam, addition of the appropriate phase profile to an existing kinoform can also transform single optical traps or complete patterns of traps into virtually any of the variants of the conventional optical tweezers discussed in section 3 above. Figure 27 shows an array of identical optical vortices (fig. 27.a.) as well as an array of vortices with varying topologi-cal charge *l* (fig. 27.b.) obtained using this method28. Fig. 27.c. shows several colloidal polystyrene spheres trapped on the bright circumferences of 9 optical vortices with *l* = 15.

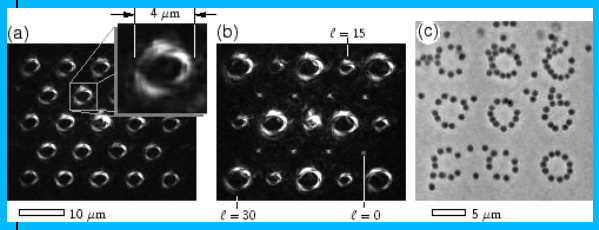

*Figure 27: **a**. Triangular array of optical vortices with topological charge l = 20. The inset shows a single one of these vortices enlarged. **b**. Similar array of vortices, where the topological charges of individual optical vortices are independently varied between values of l = 0, 15 and 30. (Light from*

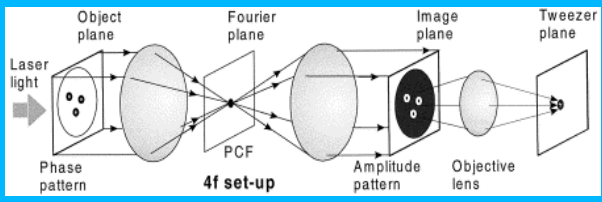

*the focused optical vortices is imaged through reflec-tion off a mirror in the focal plane.) **c**. Multiple, 0.8 μm in diameter polystyrene particles trapped on the bright circumferences of l =15 optical vortices in a 3x3 array.28*

Dynamic holographic optical tweezers arrays thus offer the possibility to dynamically form and reconfigure 3D trapping structures, consisting of any combination of the individual optical traps discussed above. Drawbacks of this technique are however, the need to calculate the necessary phase holograms beforehand, for every slight translation of a single optical trap, and the reduced trapping efficiency, which is a result of possible optical losses into unwanted diffraction orders due to the use of a pixelated SLM.

4. III. Generalized phase contrast trapping

The generalized phase contrast (GPC) technique is a variation on the dynamic HOT method described in the previous section. Instead of making use of computer-generated holograms to create arbitrary

trapping patterns, the GPC technique converts the spatial phase profile across an SLM's interface directly into the corresponding spatial intensity distribution in the focal plane of objective lens[31]. As its name implies, the GPC technique is a generalization of the well-known phase contrast technique discovered by the Dutch scientist F. Zernike[32].

In the set-up (so-called 4*f* set-up) for this technique, an expanded, monochromatic collimated laser beam of wavelength λ is incident on a phase-only liquid-crystal SLM. The SLM, located at the object plane of the 4*f* set-up (fig. 28.), encodes the desired spatial profile in the phase component of the incident beam, which is then focused onto a phase contrast filter (PCF) located in the Fourier plane of the 4*f* set-up by a lens. The PCF consists of a 60 μm diameter hole in an in the visible region non-absorbing ITO (indium tin oxide) layer of λ/2 thickness, deposited on a glass plate. Consequently, the difference in refractive index between the ITO-layer and the air-filled hole acts as a simple phase shifting filter. The PCF thus behaves as a path interferometer; it phase shifts the lower spatial frequency components of the incident beam with respect to its higher spatial frequency components. The phase shifted lower spatial frequency component of the wavefront then serves as a synthetic reference wave for the higher frequency components. Detailed and more quantative descriptions of the PCF operation have been made previously[33,34].

Figure 28: The imaging system employed for the generation of optical tweezers arrays using the GPC technique. The phase-only spatial light modulator, located in the object plane of the 4f set-up, induces a phase pattern in the incident light. The phase pattern is converted into the corres-ponding intensity profile in the image plane of the 4f imaging system by the implementation of a phase contrast filter(PCF) in its Fourier plane. An objective lens finally reduces and focuses the desired intensity pattern in its focal plane, creating the desired pattern of optical traps.31

Effectively, after passing through another lens, the spatial intensity distribution of the light in the image plane of the system corresponds spatially to its imposed phase profile in the object plane of the system (fig. 28). Finally, a microscope objective lens is used to downscale and focus the obtained intensity profile its focal plane (tweezer plane). The direct imaging between the SLM and the intensity profile in the tweezer plane is the feature which renders this technique highly effective, since it excludes the requirement of recalculating a hologram for each reconfiguration. In fact, by optically adressing the phase-only SLM using the video signal from a standard personal computer, the positions of multiple optical traps can be reconfigured in real-time 'by the click of a mouse'.

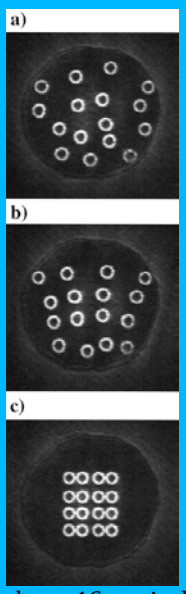

*Figure 29: Sequential images of the dynamic reconfiguration of a trapping pattern, recorded by a CCD camera located at the focal plane of the GPC optical tweezers system. A disordered pattern of 16 optical vortices (**a**.) is dynamically translated and aligned (**b**.) to form an ordered 4x4 array of optical traps (**c**.).31*

The GPC method has been used to create arrays of optical vortices31, as depicted in fig. 29. The sequential images show how 16 optical vortices are independently translated and aligned to form a 4x4 array of optical traps. Removal of the PCF or the SLM from the set-up results in uniform illumination in the focal plane of the objective lens.

This technique is capable of creating an arbitrary number of optical traps in an arbitrary configuration and manipula-ting them individually as well as groupwise at video frame rates. Additionally, any kind of optical trap described in section 3 can be generated, as well as any combination of them. The GPC method uses a non-pixelated SLM, which excludes possible optical losses into higher diffraction orders. This and the other advantages, mentioned previously, which the GPC technique has over the dynamic HOT technique, is contrasted by its limitation to the generation of 2D trapping patterns. Nevertheless, the GPC method has shown its usefullness in the fast organization of small objects in thin samples[35].

4. IV Applications of multiple dynamic tweezers

This section will treat just a few illustrative examples of the applications of multiple optical tweezers, since it is virtually impossible to give a complete overview of the uses of this rapidly growing field of science. Since this paper focuses on the potential and applications of optical tweezing techniques in micromechanics and micro-engineering, the examples given here have been selected to indicate the usefulness of multiple optical tweezers in these two sub-branches of the field.

Multiple, dynamic optical tweezers have been applied to create optically driven microfluidic pumps and valves[36,37]. In these microfluidic

devices, multiple colloidal silica spheres are manipulated using the scanned time-shared optical tweezers technique. The manipulation can however, also be achieved by the other multiple tweezing techniques capable of creating dynamic 2D patterns (dynamic HOT and GPC technique). Two types of pumps have been developed, based on positive-displacement pumping techniques. The first design consists of two 'lobes', both consisting of two colloidal 3-µm silica spheres, that are rotating in opposite directions (fig. 30). The two lobes are optically trapped and rotated in a broadened section of a microfluidic channel, which has been created using soft photolithography techniques[38]. By optically inducing clockwise rotation of the top lobe and counterclockwise rotation of the bottom lobe using the time-shared laser scanning technique, a laminar flow from left to right is created. The flow direction can be easily reversed by reversing the rotation directions of both lobes.

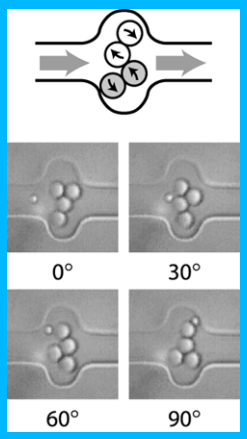

Figure 30: Pump design consisting of two lobes rotating in opposite directions, thereby inducing a microfluidic flow from left to right. A tracer particles was added to visualize the fluid flow, the four sequential photographs show frames separated by two cycles of the 2 Hz lobe rotation.36

The second pump design is based on the optically induced peristaltic movement of a string of colloidal 3-µm silica spheres (fig. 31). The colloids are moved across a microfluidic channel (created by soft-lithography techniques) in a cooperative manner, thereby inducing a 'snake-like' motion of the string of colloids. Using the time-shared laser scanning technique to move the colloids in a propagating sine wave, a flow from right to left is created. The flow direction can easily be reversed by changing the propagation direction of the colloidal wave movement.

Using the same methods, a micromechanical valve has been created. The valve consists of a 3-µm silica sphere attached to a linear chain of several 0.64-µm silica spheres. All spheres have been glued into one structure by photopolymerization, thereby forming a 2D flap-valve. Incorporation of the valve in a forked microfluidic channel creates a sorting device (fig 32.). Flapping the valve using a dynamic optical trap alternately closes the top or bottom exit channel, guiding the particle flow into the open channel.

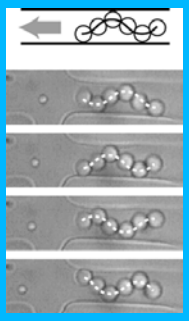

Figure 31: Peristaltic pump inducing a right to left flow by moving a string of colloidal silica spheres in a propagating sine wave at 2 Hz. A tracer particle has been added to visualize the microfluidic flow. The four sequential frames shown are separated by four cycles.36

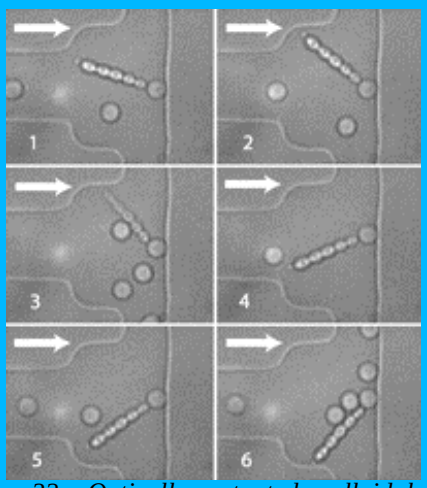

Figure 32: Optically actuated colloidal valve. Frames 1-3 show the valve being flipped to close the top channel, thereby directing the particle flow into the bottom channel. Frames 4-6 show the valve being moved to close the bottom channel, which results in a particle flow into the top channel.36

Applications of multiple dynamic optical tweezers in micro-mechanics and microscopic engineering such as the examples treated here even further increase the potential of the optical trapping technique to create optically driven, complex micromachines.

5. Conclusions

Since the first single-beam gradient force optical trap was built, almost two decades ago, the optical trapping technique has been applied in virtually all natural sciences. The field has made a huge progress in versatility and applicability throughout the years. Where conventional optical tweezers can be applied to trap transparent microscopic objects that have a higher refractive index than their surroundings, optical vortices can be applied to trap dark-seeking or photosensitive objects such as absorbing, reflecting or low-dielectric-constant particles. These optical vortices are however, only

capable of 2D optical trapping, which causes the need to incorporate axial constraints in the trapping set-up to ensure 3D confinement of objects. Although their ability to exert optical torques as well as optical forces has proven very usefull in studies of the orbital angular momentum of light, using optical vortices for particle rotation is limited to the small range of non-photo-sensitive particles that are transparent enough to allow for optical trapping, while absorbing enough light to be optically rotated. Optically induced rotation of prefabricated helical structures using conventional optical tweezers is even more limited in material choice, but it does allow for controlled optical rotation of micromechanical structures. The by far fastest class of optical rotators is restricted to particles of birefringent materials, which simultaneously indicates its main disadvantage. The rotating trapping pattern technique allows for the rotation of the widest variety of particles, but the optical rotation frequency is limited to a few Hz. In general, one can state that the best technique for optical rotation depends on the specifics of the system.

At present day, optical trapping is still a hot topic in the research community, as indicated by the many optical-tweezers-related publications in the last few years. Recently, various methods have been developed to simultaneously generate and dynamically reconfigure multiple optical traps. Using scanned time-shared optical traps, computer-controlled trapping patterns can be generated and dynamically reconfigured in a straightforward way. The trapping patterns that can be created in this way are however, limited to not too extensive 2D patterns consisting of connected lines. Dynamic holographic optical tweezers are capable of creating much more extensive and complex 3D trapping patterns that do not necessarily consist of connected lines, but any slight reconfiguration of the pattern requires the pre-calculation of a corresponding phase hologram through a complex iterative procedure. Such sophisticated and complex calculations are not necessary in the generalized phase contrast approach, where an arbitrary phase pattern is directly converted into the corresponding intensity pattern in the trapping plane. However, also the GPC technique is currently limited to the creation of 2D patterns. Since all the multiple trap techniques are in principle also capable of creating arbitrary patterns of the discussed optical trapping variants, one can say that the GPC method seems to be the superior of the three methods where 2D trapping patterns are concerned, while currently only the dynamic HOT technique enables the generation and reconfiguration of 3D patterns.

In conclusion, it can safely be stated that the scientific field of optical trapping is still blooming. The field has gotten a renewed impuls and a great deal of scientific attention since the invention of multiple dynamically reconfigurable optical traps. The examples of its applications discussed in this paper mark what is most probably only the beginning of its potential being realized. Next to the usefulness optical trapping will surely have in fundamental research, its non-invasive ability to control many microscopic objects at once will continue to be used for the exploration of its many possibilities. Through the formation and operation of functional micromechanical machines, optical trapping techniques should speed up the development of lab-on-a-chip technologies. Even without considering its biological and medical potential, the narrow, bright focus of an optical trap has a broad scientific future, which is at least as bright.

Appendix

In section 2 a qualitative description of the optical trapping in the Mie regime ($d >> \lambda$) is given. To get a feeling for the magnitude of the optical forces that are exerted on a Mie particle in an optical trap, a more quantitative description is outlined in this appendix. Many of the applications of optical tweezers deal with the optical confinement of micron-sized objects, which are in the Mie regime. As mentioned in section 2, in the Mie regime one can apply simple ray optics to the problem and decompose the incident laser beam in individual rays. Each ray in the laser beam has its own intensity, direction and polarization state and each ray propagates in a straight line in a medium of uniform refraction index. The model for the optical trap in the Mie regime is schematically depicted in fig. 33. The incident beam consisting of parallel rays enters the circular input aperture (radius r_{max}) of a high numerical aperture (N.A.) microscope objective lens. The direction of propagation of the incident beam is defined as the z-axis and the center of a dielectric micron-sized particle is defined as the origin of the coordinate system. The microscope objective is placed above the particle, in a transverse plane. Each individual ray enters the objective at an arbitrary distance r from the z-axis and at an arbitrary angle β with respect to the y-axis, and is focused to the dimensionless focal point f. The finite size of the focal spot, which is of the order of the wavelength (λ) of the incident light, can be neglected since the trapped particle is of much larger dimension than λ in this regime. The convergence angle of the rays is given by ϕ and is maximum for rays incident on the edge of the aperture. For example, for an objective lens of numerical aperture value N.A. = 1.25, the maximum convergence angle ϕ_{max} is equal to 70°, for a ray entering the numerical aperture at r_{max}.

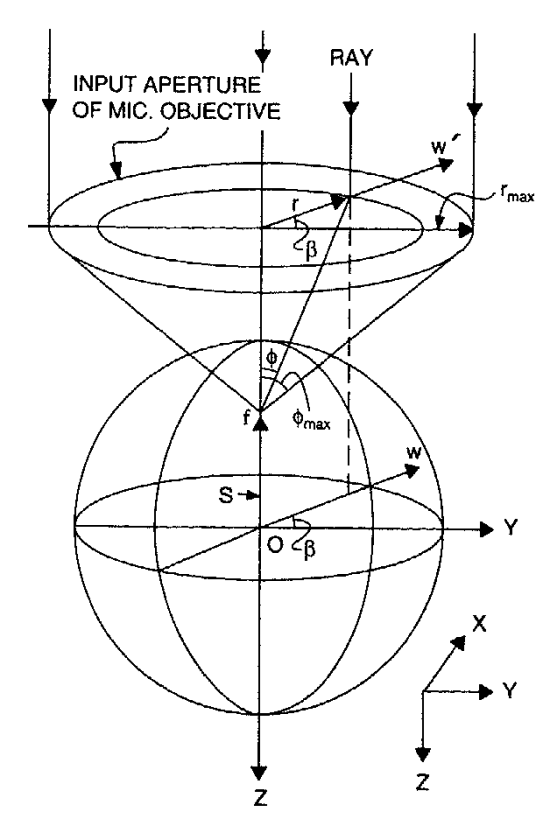

Figure 33: Schematic drawing of the model used to calculate optical forces in the Mie regime. The incident laser beam is decomposed into separate rays which are individually focussed to a dimensionless focal point using a high numerical aperture lens.[39]

Consider the force that is exerted on the particle when a single ray of power P is incident on the particle at an angle of incidence θ with respect to the surface normal (see fig. 34). The ray, traveling in the z direction, carries an incident momentum per second of n_1P/c, where n_1 is the index of refraction of the medium surrounding the particle and c is the speed of light in vacuum. The incident ray is partially reflected and partially refracted by the particle, resulting in an infinite series of scattered rays of decreasing power. The reflected ray makes an angle of $\pi+2\theta$ with the incident ray direction and has power PR, the ray that goes straight through the particle emerges at an angle α and has power PT^2 and subsequent emergent rays come out at an angle $\alpha+k\beta$ having power PT^2R^k, where k is the number of internal reflections the correspondings ray has undergone. The quantities R and T are the Fresnel coefficients of reflection and transmission of the particle's surface at incident angle θ, respectively. The total force exerted on the origin of the particle is the net change in momentum per second of the incident ray, which is a sum over the contributions of the infinite number of emergent rays.

Figure 34: Schematic drawing of the scattering of a single incident ray by a dielectric sphere in a top view. The incident ray is partially reflected and scattered, resulting in an infinite series of rays of decreasing power emerging from the particle.[39]

The change in momentum per second in the z direction due to all the emergent rays gives the total force in the z direction:

$$F_z = \frac{n_1 P}{c} - \frac{n_1 PR}{c}\cos(\pi + 2\theta) - \sum_{k=0}^{\infty} \frac{n_1 PT^2}{c} R^k \cos(\alpha + k\beta) \qquad \text{(A1)}$$

Similarly, the total force in the y direction is given by the net momentum change in this direction:

$$F_y = -\frac{n_1 PR}{c}\sin(\pi + 2\theta) - \sum_{k=0}^{\infty} \frac{n_1 PT^2}{c} R^k \sin(\alpha + k\beta) \qquad \text{(A2)}$$

The forces exerted on the particle can be simplified by considering the total force in the complex plane[39], $F_{tot} = F_z + iF_y$. In the complex plane the total force is given by:

$$F_{tot} = \frac{n_1 P}{c}[1 + R\cos(2\theta) + iR\sin(2\theta)] - \frac{n_1 PT^2}{c}\sum_{k=0}^{\infty} R^k e^{i(\alpha+k\beta)} \qquad \text{(A3)}$$

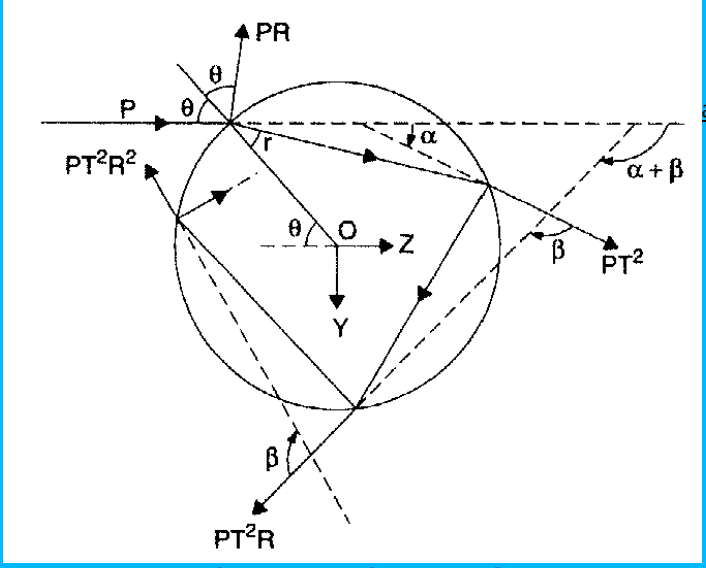

Now the sum over *k* is a simple geometric series with the general solution:

$$\sum_{x=0}^{\infty} y^x = \frac{1}{1-y} \tag{A4}$$

This gives for the total force:

$$F_{tot} = \frac{n_1 P}{c}[1 + R\cos(2\theta) + iR\sin(2\theta)] - \frac{n_1 P T^2 e^{i\alpha}}{c(1 - \mathrm{Re}^{i\beta})} \tag{A5}$$

One can separate the imaginary and real parts of eq. A5 by rationalizing the complex denominator and simplify the expression using the goniometric sum and difference relations *sin(x-y)=sin(x)cos(y)-cos(x)sin(y)* and *cos(x-y)=cos(x)cos(y)-sin(x)sin(y)*, which yields:

$$F_{tot} = \frac{n_1 P}{c}[1 + R\cos(2\theta) - \frac{T^2(\cos(\alpha) - R\cos(\alpha - \beta))}{R^2 - 2R\cos(\beta) + 1}] + i\frac{n_1 P}{c}[R\sin(2\theta) - \frac{T^2(\sin(\alpha) + R\sin(\beta - \alpha))}{R^2 - 2R\cos(\beta) + 1}] \tag{A6}$$

Using the geometric relations $\alpha = 2\theta - 2r$ and $\beta = \pi - 2r$ (see fig. 34), where θ and r are the angles of incidence and refraction of each ray, respectively, the force forces in the z direction (real part of eq. A6) and in the y direction (imaginary part of eq. A6) can be rewritten. The force exerted in the z direction is the scattering force for this single ray, defined as the component of the total force along the direction of propagation of the incident ray.

$$F_z = F_{scat} = \frac{n_1 P}{c}[1 + R\cos(2\theta) - \frac{T^2(\cos(2\theta - 2r) + R\cos(2\theta))}{R^2 + 2R\cos(2r) + 1}] \tag{A7}$$

The force in the y direction then corresponds to the gradient force that this single ray exerts on the particle, defined as the component of the total force along the direction perpendicular to the incident ray's path:

$$F_y = F_{gr} = \frac{n_1 P}{c}[R\sin(2\theta) - \frac{T^2(\sin(2\theta - 2r) + R\sin(2\theta))}{R^2 + 2R\cos(2r) + 1}] \tag{A8}$$

To get a feeling for the magnitude of the optical forces exerted on a particle, consider the forces that are exerted on a polystyrene sphere in water (n_1 = 1.33) when a ray of 10mW power is incident on the particle at an angle of θ = 40°. The index of refraction of polystyrene, n_2 , is 1.6. According to Snell's law the angle of refraction is in that case equal to r = 32.3°. Assuming values of 0.1 and 0.9 for the reflection (R) and transmission (T) coefficients, respectively, the forces acting on the particle are:

$$F_y = F_{grad} = -0.76\frac{pJ}{m} = -0.76\,pN$$

As expected in from qualitative picture in section 2, the force in the y-direction is negative, meaning the particle's center is pulled towards the highest intensity point, which in this case is the single ray. The typical optical forces exerted on a particle are in the pico-Newton-range, which can is also evident from eqs. A7 and A8; *R*, *T* and all the cosine and sine values can only take values between 0 and 1, meaning the quantity between brackets in both equations is of order of 1, while n_1P/c is of piconewton order in this case. Of course, the forces exerted are linearly proportional to the power of the incident ray, so by increasing the incident laser power the exerted forces increase accordingly. This model assumed the refractive index of the particle to have no imaginary part, meaning it does not absorb any light. In reality however, particles will almost always absorb some portion of the incident light, so at some point the increased power is sure to damage the trapped particle, which limits the force that can be exerted on the particle. An

optimum can be found by varying the wavelength of the incident light, but in this case one has to keep in mind that n, R,T and indirectly r also vary with λ.

Of course, the above expressions only give the forces on a spherical particle exerted by a single ray. To calculate the net force exerted on a trapped particle, which is the vector sum of all the forces exerted by all the incident rays. This can be and has been done39 by relating the angle of incidence, θ, of each ray to the position at which it enters the numerical aperture (r,β in fig. 33) and integrating numerically over the proper distribution of rays in the incident laser beam (a Gaussian distribution, for example, for a Gaussian incident beam).

[1] Grier, D. G. A revolution in optical manipulation. *Nature* **424,** 810-816 (2003)

[2] Dholakia, K., Spalding, G. & MacDonald, M. Optical tweezers: the next generation. *Phys. World.* **31** (2002).

[3] Ashkin, A. History of optical trapping and manipulation of small-neutral particles, atoms, and molecules. *IEEE J. Sel. Top. Quantum Elec.* **6**, 841-856 (2000)

[4] Ashkin, A. Acceleration and trapping of particles by radiation pressure *Phys. Rev. Lett.* **24**, 156-159 (1970)

[5] http://www.jb.man.ac.uk/atlas/gloss.html

[6] http://www.biop.dk/Research/Tweezers.htm

[7] Harada Y. & Asakura T. Radiation forces on a dielectric sphere in the Rayleigh scattering regime. *Opt. Commun.* **124**, 529-541 (1996)

[8] Kawata, S. *et al.* Finer features for functional microdevices. *Nature* **412**, 697-698 (2001)

[9] Mauro, S. Nakamura, O. & Kawata, S. Three-dimensional microfabrication with two-photon-absorbed photopolymerization. *Opt. Lett*. **22**, 132-134 (1997)

[10] Cumpston, B.H. et al. Two-photon polymerization initiators for three-dimensional optical data storage and microfabrication. Nature **398**, 51-54 (1999)

[11] Galajda, P. & Ormos, P. Complex micromachines produced and driven by light. *Appl. Phys. Lett.* **78**, 249-251 (2001)

[12] Allen, L. *et al.* Orbital angular-momentum of light and the transformation of Laguerre-Gaussian laser modes. *Phys. Rev. A* **45**, 8185-8189 (1992)

[13] http://departments.colgate.edu/physics/research/optics/oamgp/gp.htm

[14] Rubinzstein-Dunlop, H. *et al.* Optical trapping of absorbing particles. *Adv. Quantum Chem.* **30**, 469-492 (1998)

[15] O'Neill, A.T. & Padgett, M.J. Three-dimensional optical confinement of micron-sized metal particles and the decoupling of the spin and orbital angular momentum within an optical spanner. *Opt. Commun.* **185**, 139-143 (2000)

[16] Gahagan, K.T. & Swartzlander, G.A. Trapping of low-index microparticles in an optical vortex. *J. Opt. Soc. Am. B* **15**, 524-534 (1998)

[17] Curtis, J.E. & Grier, D.G. Structure of optical vortices. *Phys Rev. Lett.* **90**, 133901 (2003)

[18] Allen, L., Padgett, M.J. & Babiker, M. The orbital angular momentum of light. *Prog. Opt*. **39**, 291-372 (1999)

[19] Beth, R.A. Mechanical detection and measurement of the angular momentum of light. *Phys. Rev.* **50**, 115-125 (1936)

[20] Friese, M.E.J. *et al.* Optical alignment and spinning of laser-trapped microscopic particles. *Nature* **394**, 348-350 (1998)

[21] Paterson, L. *et al*. Controlled rotation of optically trapped microscopic particles. *Science* **292**, 912-914 (2001)

[22] Courtial, J. Self-imaging beams and the Guoy effect. *Opt. Commun.* **151** 1-4 (1998)

[23] Arlt, J. & Padgett, M.J. Generation of a beam with a dark focus surrounded by regions of higher intensity: The optical bottle beam. *Opt. Lett.* **25**, 191-193 (2000)

[24] Sasaki, K. *et al*. Pattern formation and flow control of fine particles by laser-scanning micromanipulation. *Opt. Lett.* **16**, 1463-1465 (1991)

[25] Mio. C. *et al.* Design of a scanning laser optical trap for multiparticle manipulation. *Rev. Sci. Instrum.* **71**, 2196-2200 (2000)

[26] Dufresne, E.R. *et al.* Computer-generated holographic optical tweezers arrays. *Rev. Sci. Instr*. **72**, 1810-1816 (2001)

[27] Liesener, J. *et al*. Multi-functional optical tweezers using computer-generated holograms. *Opt. Commun.* **185**, 77-82 (2000)

[28] Curtis, J. E., Koss, B.A. & Grier, D.G. Dynamic holographic optical tweezers. *Opt. Commun.* **207**, 169-175 (2002)

[29] He, H., Heckenberg, N.R. & Rubinsztein-Dunlop, J. Optical particle trapping with higher-order doughnut beams produced using high efficiency computer generated holograms. *J. Mod. Opt.* **42**, 217-223 (1995)

[30] Reicherter, M. *et al.* Optical particle trapping with computer generated holograms written on a liquid-crystal display. *Opt. Lett.* **24**, 608-610 (1999)

[31] Mogensen, P.C. & Glückstad, J. Dynamic array generation and pattern formation for optical tweezers. *Opt. Commun*. **175**, 75-81 (2000)

[32] Zernike, F. How I discovered phase contrast. S*cience* **121**, 345-349 (1955)

[33] Glückstad, J. Phase contrast image synthesis. *Opt. Commun.* **130**, 225-230 (1996)

[34] Glückstad, J. Pattern generation by inverse phase contrast. *Opt. Commun*. **147**, 16-18 (1998)

[35] Rodrigo, P.J. *et al.* Interactive light-driven and parallel manipulation of inhomogeneous particles. *Opt. Exp*. **10**, 1550-1556 (2002)

[36] Terray, A., Oakey, J. & Marr, D. W. M. Microfluidic control using colloidal devices. *Science* **296**, 1841-1844 (2002).

[37] Terray, A., Oakey, J. & Marr, D. W. M. Fabrication of linear colloidal structures for microfluidic applications. *Appl. Phys. Lett.* **81**, 1555-1557 (2002).

[38] Whitesides, G. M. & Stroock, A. D. Flexible Methods for Microfluidics. *Phys. Today* **54**, 42-49 (2001).

[39] Ashkin, A. Forces of a single-beam gradient trap on a dielectric sphere in the ray optics regime. *Biophys. J.* **61**, 569-582 (1992)